The Geometric Localization of STEREO CMEs

V J Pizzo and D A Biesecker

NOAA Space Environment Center

325 Broadway

Boulder, CO 80305

Abstract. We describe a straightforward methodology for determining the location and other gross properties of CMEs within the coronagraph field of view in the upcoming STEREO mission observations. We use geometric triangulation upon a series of lines-of-sight taken from two spacecraft views that are locally tangent to the apparent edges of a CME. From the intersections of these lines-of-sight, we construct a set of stacked quadrilaterals that fully bound the structure and convey something of its location, shape, and size; a time sequence of such determinations can be used to determine the velocity. The technique is relatively robust and promises a substantial improvement in our capability to locate and characterize CMEs for research as well as forecasting purposes.

Index terms: 2111, 2169, 7513, 7594

Keywords: coronal mass ejections, stereoscopic image analysis, space weather forecast tools

1. Introduction

White light imagery from the upcoming STEREO mission presents a unique opportunity to obtain reliable estimates of CME location, shape, and velocity. In addition to the obvious space weather forecast applications, accurate knowledge of these gross CME properties is certain to open up entire new vistas of understanding in terms of associations among solar surface, coronal, and interplanetary structures and disturbances.

Realizing the full promise of the twin stereo views will not be a simple task. A variety of methods are being explored to exploit STEREO image data, including tomographic deconvolution (eg., *Davila*, 1994; *Zidowitz et al*., 1996; *Newmark et al*., 2003; *Hick and Jackson*, 2003), tie-point analysis (P. Liewer *et al., private communication*), and, most recently, polarization studies (*Moran and Davila*, 2004).

Whatever the ultimate potential of these methods, there is a need within the space weather community for a means to determine quickly and accurately the gross properties of Earth-directed CMEs. Moreover, there is specific need for a near-real-time forecasting tool that can routinely and confidently be applied to the real-time, low-resolution "beacon" data stream. Ideally, such a tool would work with either the coronagraph or the heliospheric imager beacon data. Simplicity, robustness, and ease of use would be an issue, since the CME locator algorithm would have to run in automated or nearly automated mode within a forecast center. As a dividend, the resultant archive of CME properties would have clear and immediate relevance to broader research investigations.

We describe a straightforward methodology that meets the above requirements. Although it does not yield the structural details that other methods may potentially deliver, it nonetheless constitutes an enormous improvement over current capabilities, on both forecasting and research-

oriented fronts. Most importantly, it is a method that can unquestionably be made fully ready for operation before launch. While its utility is lessened at very small and very large angular separations of the twin STEREO spacecraft, it can be applied successfully over most of the core mission.

We focus upon CMEs in the corona, where they are most compact and where there exists lengthy experience in analyzing and interpreting transient disturbances. We describe here the results of a proof-of-concept study based upon geometric triangulation. Specifically, by determining from two spacecraft views a series of lines-of-sight that are locally tangent to the apparent edges of a CME it is possible to construct a set of stacked quadrilaterals that bound the structure. The assemblage of quadrilaterals can be used to estimate the geometric centroid of the disturbance and also to convey something of its shape and orientation. Among the strengths of the method is the fact that it is contingent only upon discerning the outlines of the configuration, ensuring robustness in the face of coarse, noisy images and making it amenable to automation via standard edge-detection techniques.

2. Forward Modeling

A forward modeling environment is used to develop, test, and illustrate the geometric localization technique. The modeling employs several key elements to support the simulation and analysis of white light observations in the corona.

2.1. Simplified Sun-Earth coordinate system.

The coordinate system we use for development is illustrated in Figure 1, which shows a heliocentric Cartesian system (“HC”) linked to a geocentric Cartesian system (“E”). Here, we neglect the relative tilts of the solar and ecliptic polar axes; thus, Z_{HC} is parallel to Z_{E}. As needed, points defining CME, spacecraft, or other locations are expressed in either heliocentric

or geocentric systems, in either Cartesian or spherical coordinates. Thus, points along the lines of sight from either spacecraft [e.g., (η_{A1},λ_{A1})] may be readily transformed from one system to another to facilitate line-of-sight (LOS) evaluations.

2.2. Parameterized representations of ambient and transient coronal density structures.

The coronal density, including both ambient and CME components, is discretized in a regularly gridded spherical shell running between 1 R_S and a specified outer boundary, lying typically at 10-20 R_S. The *Guhathakurta et al.* (1996) tilted-dipole model provides the background coronal density distribution. The tilt and orientation of the model current sheet structure are adjustable via parameters.

CMEs are modeled as simple, ad hoc, teardrop-shaped density configurations derived from cosine-based expressions. Density distributions for the CME are specified in terms of a streamline function ψ, which is a function of distance from the origin, ρ, the angle from the model CME axis, ζ, and a factor controlling the CME shape, p:

$$\psi(\rho, \zeta) = (1 / \rho) \times \cos^{(p/2)}(2\zeta) \qquad (1)$$

The spatial configurations of surfaces of constant ψ for several (p, ρ) combinations are shown in Figure 2. The values of ψ are inversely related to the maximum axial extension of the CME configuration, whereas the angular width is a function of p. Hence it is possible to define a dense shell CME by specifying p, identifying $\psi_{outer}=1/\rho_{outer}$ and $\psi_{inner}=1/\rho_{inner}$, and then setting all points lying within the shell ($\psi_{outer} < \psi < \psi_{inner}$) to some specified density. All points interior to ψ_{inner} are set to some low value to simulate the CME cavity. In this implementation, the CME density is fixed by specifying at each included grid point the ratio to a reference density profile, which is given as a function of ψ and heliocentric distance. Also, by specifying p as a function of

angle about the CME axis, the CME cross-section can be elongated in some chosen direction relative to the solar equator.

Finally, the model CME configuration is embedded into the gridded coronal density structure by replacing all local ambient values with the model CME values. Dynamical interactions between the CME and the ambient corona are thus explicitly neglected.

2.3. Synthetic white light imagery.

We have set up an LOS integration based upon the *Billings* (1966) formulation for coronal scattering, as articulated by *Hundhausen* (1993). The coronal density at each discrete point along an LOS is linearly interpolated (in the log) from the gridded density distribution. The limb-darkening function u is assumed to be 0.5. Adequate spatial resolution along each LOS is verified to assure accurate calculation of both tangential and radial polarization components.

3. Geometric Localization

The geometric localization technique as described below currently requires manual operation, but the possibilities for automation should be self-evident. The basic idea is to obtain four LOS's – two from each spacecraft – each being tangent to a perceived edge of the CME in the two white light images and, importantly, all lying within a common plane. Figure 1 shows the LOS's needed to bound a slice through a generic CME structure, with the quadrilateral formed by their mutual intersections being depicted by the heavy lines.

Figure 3 shows a synthetic white light image pair simulating a STEREO-like coronagraph observation of a model CME. It is centered 15° to the west of the Sun-Earth line, and 15° north of the heliocentric equator. It is also elongated (oblate cross-section) in a direction that is inclined some 30° to a north-south line, with the northernmost portions of the structure lying to the west of the southern part of the structure. The local density enhancement within the CME

shell is arbitrarily concentrated toward the leading edge of the overall disturbance. The two simulated spacecraft views assume the spacecraft are in 1 AU orbit, with Figure 3 (left) showing the apparition from a position leading Earth by 35°, the other (right) from a 35° trailing location. Thus the net spacecraft separation is 70°.

The steps in the implementation are as follows:

1. On the image from spacecraft A (leading), mark a point along the western edge of the CME. Together with a line connecting the two spacecraft, this LOS (L_{A1}) defines a plane in three-space. To obtain the 3D equation of the L_{A1}, we posit a ghost point *q* lying 1 AU from spacecraft A along the direction given by the longitudinal and latitudinal elongation angles η_{A1} and $\lambda_{A1.}$ From the known heliocentric locations of the spacecraft and the point *q*, we evaluate the constants {*A, B, C*} in the 3D line equation

$$\frac{(x - x_q)}{A} = \frac{(y - y_q)}{B} = \frac{(z - z_q)}{C}. \qquad (2)$$

2. On this same image, display the intersection of the plane containing the two spacecraft and L_{A1}, as viewed from the spacecraft A. This is accomplished by using Eq. (2) to define a line running from *q* over to the heliocentric location of spacecraft B (lagging). A sufficient span of the plane is drawn across the field of view that it includes the first point and cuts completely across the CME through its eastern edge.
3. Define a second LOS (L_{A2}) tangent to the eastern limb of the CME, also lying in the common plane.
4. On the view from spacecraft B, draw the plane including L_{A1} and $L_{A2,}$ such that it cuts completely across the CME. Identify two new LOS's (L_{B1}, tangent to the western edge, and L_{B2}, tangent to the eastern edge) lying in this plane, and obtain the 3D line constants.

5. From the four LOS's, determine by triangulation the four intersection points. These define a quadrilateral bounding a thin slice through the CME.
6. Repeat steps 2-5 above for a succession of thin slices through the CME.

In this process, the order of the LOS's is immaterial, and one would generally choose for the first LOS the spacecraft view and CME limb offering the most distinct edge. The number of slices taken should be commensurate with the inherent north-south spatial resolution. The slices are nearly horizontal because both spacecraft lie in the ecliptic and are relatively far from the Sun. It should also be noted that geometric localization differs from the tie-point approach in that while the tangent direction is determined observationally, the actual tangent point to the CME along an LOS is irrelevant: all that matters are the intersections of the LOS's that define the four corners of the quadrilateral.

The amalgam of all these slices defines a volume – which we refer to as a "bounding box" – that encases the CME, as depicted in Figure 4. This volume can be analyzed in various ways to obtain an estimate of the CME location and its gross geometric properties. For example, it is straightforward to obtain the centroid of the bounding box, and the relative proportions of the structure, including the north-south oblateness and tilt and the radial elongation, are all evident in the shape and distribution of the bounding box lattice. The CME velocity, direction, and spatial evolution can be assessed from a time series of geometric localizations.

4. Uncertainties

A useful estimate of the systematic uncertainty in the geometric localization can be obtained by comparing for a simple model CME the area of the bounding quadrilateral with the actual area of the CME within a plane. Consider a planar slice through a spherical model CME of radius 1 R_S lying at a distance of 1 AU from two spacecraft separated by a Sun-centered angle χ.

Figure 5 shows the ratio of the quadrilateral area to the actual area. It can be seen that the bounding box places resonably tight restrictions on the CME locale over a broad range of angles, in particular those spanning the STEREO prime mission phase.

Since the accuracy of the geometric localization technique depends upon the ability to discern a well-defined edge to the structure, the subtle boundaries associated with CMEs observed very far out of the plane (i.e., an “halo” CME as seen from one STEREO spacecraft) may increase the error in the localization somewhat, even at ideal spacecraft separation angles. However, any loss of accuracy is mitigated by the fact that the geometric slices are taken in many layers spanning the entire structure. Quantification of this effect and other potential limitations associated with more complex and irregular CMEs awaits further analysis.

5. Discussion

We have developed an important tool in the arsenal for 3D analyses of upcoming STEREO data. Although it has limitations, the method described here promises a substantial improvement in our capability to locate and characterize CMEs for research as well as forecasting purposes. The method is by its geometric nature inherently robust. It can be applied to either total intensity or polarized images, perhaps without background subtraction, so long as there is sufficient contrast to define the periphery of the structure from both spacecraft. Moreover, it can be applied where other techniques, such as tomography, are impossible. For example, when part of a CME projects inside the occulting disk, one can still obtain the requisite LOS’s by visual extension of the edge of the CME, provided the underlying structure is distinct and regular enough. (This was done for the two lower slices of the example in Figures 3 and 4.) The method is thus ideal for low resolution, low cadence, near-real-time applications typifying the STEREO beacon data stream.

Because it defines reliably the overall extent and shape of a CME structure, the geometric localization technique is seen as complementary to inferences gained from the other STEREO imagery methods mentioned in the Introduction. For example, geometric localization may prove beneficial as a preliminary stage in a tomographic inversion, since it provides constraints upon the spatial domain actually occupied by the CME. In addition, it should afford useful cross-calibration of impressions of 3D CME structure gained through polarization analysis.

Finally, the technique may be applied to specific parts of a CME (e.g., the leading-edge shell, prominence material in the CME cavity, etc.), so long as the substructure has distinct boundaries.

6. References

Billings, D. W., *A Guide to the Solar Corona,* Academic, San Diego, Calif., 1966.

Davila, J. M., Solar tomography, *Astrophys. J., 423,* 871, 1994.

Guhathakurtha, M., T. E. Holzer, and R. M. MacQueen, The large-scale density structure of the solar corona and heliospheric current sheet, *Astrophys. J., 438,* 817, 1996.

Hundhausen, A. J., Sizes and locations of coronal mass ejections: SMM observations from 1980 and 1984-1989, *J. Geophys. Res., 98,* 177, 1993.

Hick, P. L., and B. V. Jackson, Heliospheric tomography: An algorithm for the reconstruction of the 3D solar wind from remote sensing observations, *Proc. of the SPIE, 5171,* 287, 2004.

Moran, T. G., and J. M. Davila, Three-dimensional polarimetric imaging of coronal mass ejections, *Science, 305,* 66, 2004.

Newmark, J. M., J. W. Cook, P. A. Reiser, and A. Yahil, 3D Electron Density Reconstruction from the SECCHI White Light Coronagraphs Onboard Stereo, (abstract only), *AAS* SPD Meeting #34, #02.02, 2003.

Zidowitz, S., B. Inhester, and A. Epple, Tomographic inversion of coronagraph images, in *Solar Wind Eight,* edited by D. Winterhalter *et al., AIP Conf. Proc., 382,* 165, 1996.

7. Figure Captions

Fig 1. Schematic of the linked Sun ("HC")- and Earth ("E")-centered coordinate systems used in the analysis. Relative tilts of the solar and ecliptic polar axes are neglected. The lines-of-sight (L_{A1}, etc.) are tangent to the respective edges of the CME, as seen by each spacecraft, and all four in each set lie in a common plane.

Fig 2. Illustration of model CME configurations, for various values of the parameters p and ρ in Eq. (1). Surfaces of constant ψ are shown for several (p, ρ) combinations, including [(3., 2.5), dotted]; [(1., 2.5), light solid]; [(1., 3.0), dark solid]; and [(5., 3.0), dashed]. For p = *const*, the shape is rotationally symmetric about the x-axis. Solar disk is indicated at left. The density enhancement (or decrement) in the CME is defined in terms of ψ and heliocentric distance. For example, the heavy solid line in the Figure can be taken to correspond to ψ_{outer} in the text, and the thin solid line to ψ_{inner}; by enhancing the density between these two surfaces, a compressive CME shell structure can be simulated.

Fig 3. Synthetic white light images showing points (asterisks) tangent to the edges of the CME and lying in a common plane (indicated by the yellow line). The CME is centered 15° north and 15° west of the Sun-Earth line. The two views are from spacecraft in 1 AU orbit leading Earth by 35° (left) and lagging by 35° (right).

Fig 4. Three views of an Earth-directed CME (green lattice) localized by five quadrilateral slices (yellow) according to the method described in the text. The radial extension of the structure, its inclined north-south elongation, and the direction of the centerline are all accurately captured by the analysis.

Fig 5. An area-based measure of uncertainty in the geometric localization technique, as a function of spacecraft separation angle. Because the triangulation object is so distant from the spacecraft, this error estimate should be meaningful for CMEs lying within ~10 R_S.

Figures

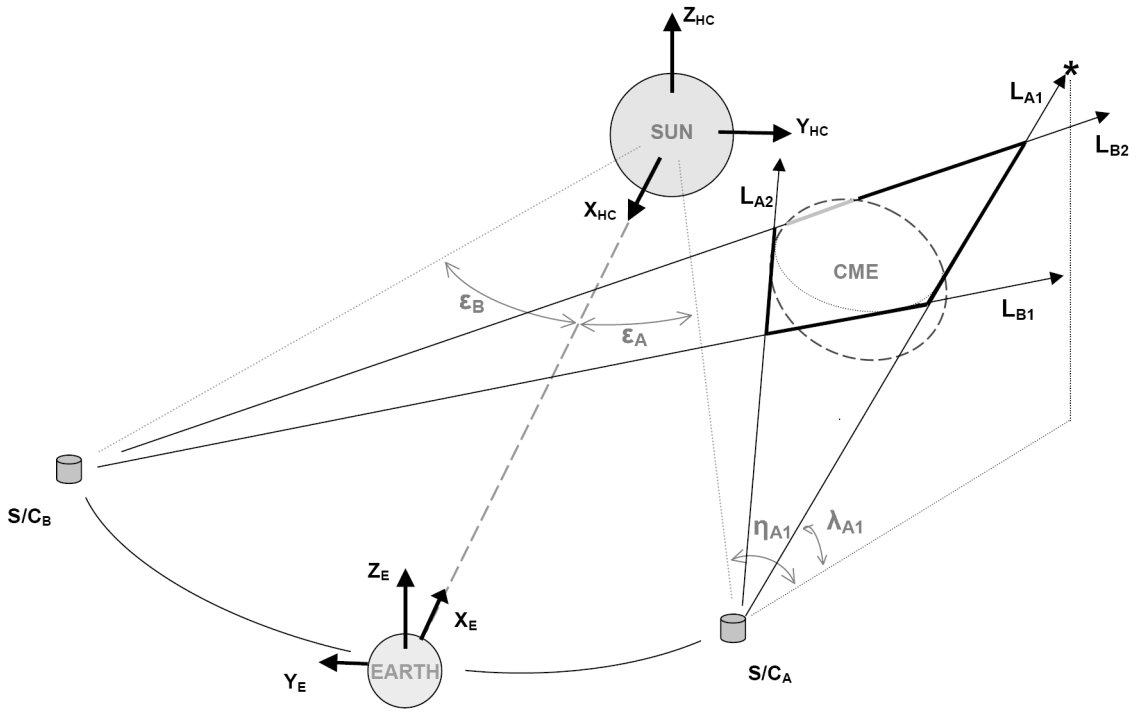

(Fig 1)

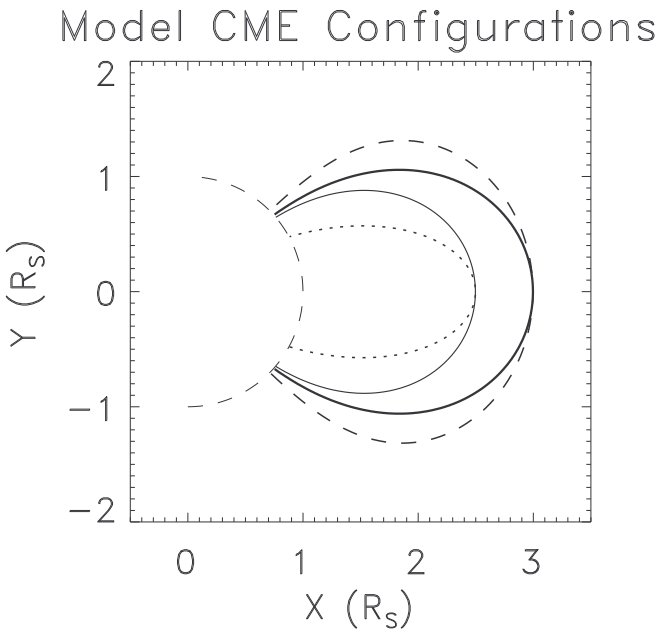
Model CME Configurations
2
1
0
−1
−2
Y (R_S)
0
1
2
3
X (R_S)

(Fig 2)

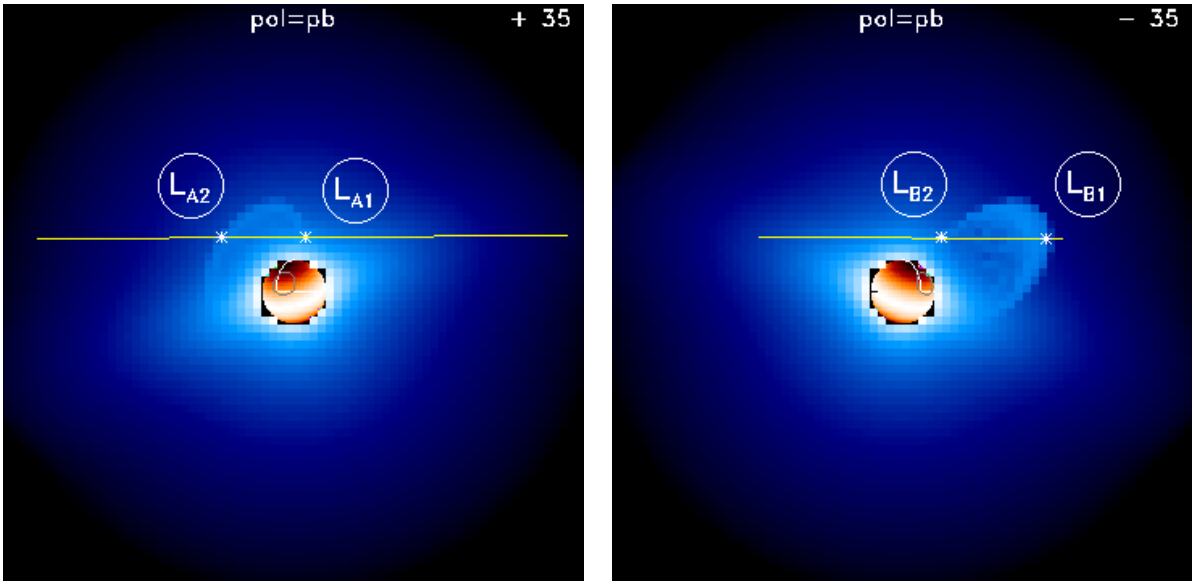
pol=pb
+ 35
L_A2
L_A1
pol=pb
− 35
L_B2
L_B1

(Fig 3)

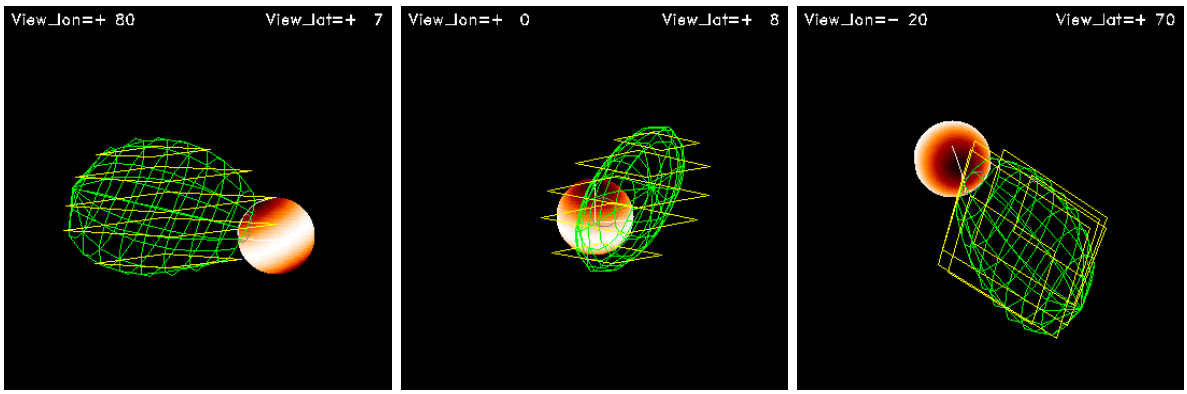
View_lon=+ 80
View_lat=+ 7
View_lon=+ 0
View_lat=+ 8
View_lon=- 20
View_lat=+ 70

(Fig 4)

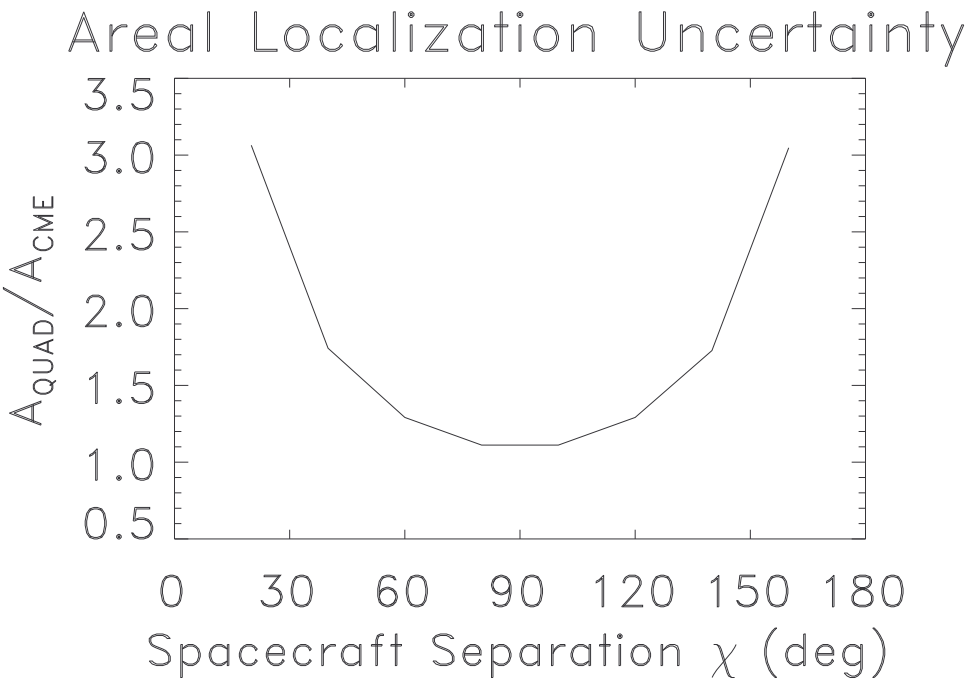
Areal Localization Uncertainty
3.5
3.0
2.5
2.0
1.5
1.0
0.5
A_{QUAD}/A_{CME}
0
30
60
90
120
150
180
Spacecraft Separation χ (deg)

(Fig 5)